

# Detailed balance in non-equilibrium dynamics of granular matter: derivation and implications

Clara C. Wanjura,<sup>1,2,\*</sup> Amelie Mayländer,<sup>3</sup> Othmar Marti,<sup>3</sup> and Raphael Blumenfeld<sup>4,5,†</sup>

<sup>1</sup>*Cavendish Laboratory, Cambridge University, JJ Thomson Avenue, Cambridge CB3 0HE, UK*

<sup>2</sup>*Max Planck Institute for the Science of Light, Staudtstraße 2, 91058 Erlangen, Germany*

<sup>3</sup>*Ulm University, Albert-Einstein-Allee 11, 89081 Ulm, Germany*

<sup>4</sup>*Gonville & Caius College, Cambridge University, Trinity St., Cambridge CB2 1TA, UK*

<sup>5</sup>*Imperial College London, London SW7 2AZ, UK*

(Dated: April 9, 2024)

Discovering fundamental principles governing the dynamics of granular media has been a long-standing challenge. Recent predictions of detailed balance steady states (DBSS), supported by experimental observations in cyclic shear experiments of planar granular systems, called into question the common belief that the detailed balance principle is only a feature of equilibrium. Here, we first show analytically that DBSS in planar granular dynamics arise when a certain conditional cell order distribution is independent of the condition. We then demonstrate that this condition is met in rotational shear experiments, which indeed also give rise to robust DBSS. This suggests that DBSS not only exist but are also quite common. We also show that, when the unconditional cell order distribution maximises the entropy, as has been found recently, then this distribution is determined by a single parameter—the ratio of splitting and merging rates of cells of any arbitrary order. These results simplify the modelling of the complex dynamics of planar granular systems to the solution of recently proposed evolution equations, demonstrating their predictive power.

**Introduction:** Modelling the dynamics of granular materials is essential to many natural phenomena and technological applications. Of particular significance is the structures into which these materials settle at the end of a quasistatic process. This structure determines many of the large-scale constitutive properties of the consolidated medium. During quasistatic dynamics of granular matter, the structure evolves by breaking and making intergranular contacts. In planar systems, the structure can be partitioned into cells, which are the smallest loops enclosed by particles. The number of particles surrounding a cell is the cell order [1]. In the following, we call a cell of order  $k$  a ‘ $k$ -cell’. Breaking a contact merges the two cells sharing it and making a contact splits a cell into two, as illustrated in Fig. 1(a). The dynamic equations,

(COD),  $Q_k(t)$  [2, 3], predict that, in very dense granular systems, the cell merging and splitting events converge to steady states that satisfy detailed balance. This prediction, which depended only on the assumption of homogeneity of  $Q_k$ , calls into question the current paradigm that: (i) only systems in thermal equilibrium satisfy detailed balance and (ii) that balance in steady states of non-equilibrium systems can only be achieved via cyclic kinetic processes, e.g., of the form  $A \rightarrow B \rightarrow C \rightarrow A$  [11]. The prediction in [1] questioned only the first statement because it is valid only for very dense systems,  $k < 6$ , that cannot have cyclic processes [12]. Such dense systems are also very difficult to realise in dynamic experiments. Nevertheless, recent experiments [13] showed that cyclically sheared much less dense granular systems also exhibit detailed balance steady states (DBSS). Finding such states in any granular system suggests that some aspects of conventional statistical mechanics can be used to model them [4]. Further support of the usefulness of statistical mechanics to granular systems is a recent finding that entropy plays a key role in the quasistatic structural organisation of granular systems [10]. They found that the COD at steady state maximises the entropy, which corresponds to maximising the number of possible cell configurations under given constraints.

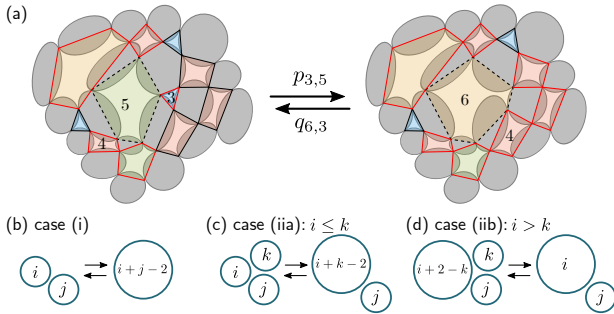


FIG. 1. **Reactions changing the number of neighbours.** (a) The merging of a 3- and a 5-cell into a 6-cell by contact breaking. Neighbouring cells share at least one contact. We show the neighbours of the central 5-cell (dashed line) on the left and the 6-cell on the right in red. (b)-(d) Different cases contributing to a change in the number of  $i$ - $j$  neighbours.

proposed recently in [1], for the cell order distribution

Here we report three main results. 1) We show analytically that DBSS *must arise* in quasistatically evolving granular systems when the conditional COD around any  $k$ -cell,  $Q_{i|k}$ , is independent of  $k$  and of position. This condition was met in the cyclic shear experiments of [13] and in our experiments, presented here. This derivation explains the observations of DBSS and suggests that they are more common in

non-equilibrium systems than currently believed. 2) We show that, if the COD in such systems also maximises the entropy, the cell merging and splitting dynamics are governed by a single protocol-dependent parameter, which also determines the entire COD. 3) We provide experimental evidence that simply sheared systems also satisfy the conditions necessary for DBSS and indeed exhibit these states. This suggests that DBSS arise in dynamics beyond cyclic shear and supports result 1. Our results show that the number of parameters required to model quasistatic dynamics of granular matter can be reduced significantly, paving the way to simpler models.

### The cell order distribution and the steady state:

The COD's evolution equations, in a planar granular system of  $N \gg 1$  particles, are [1]:

$$\begin{aligned} \dot{Q}_k = & \frac{1}{2} \sum_{i=3}^{k-1} \eta_{i,k-i+2} (1 + \delta_{i,k-i+2}) \\ & - \sum_{i=k+1}^{C-2} \eta_{k,i-k+2} (1 + \delta_{k,i-k+2}) + Q_k \sum_{\substack{i,j=3 \\ i \leq j \\ i+j-2 \leq C}} \eta_{i,j}. \end{aligned} \quad (1)$$

Here,  $\eta_{i,j} \equiv p_{i,j} Q_i Q_{j|i} - q_{i+j-2,i} Q_{i+j-2}$  is a 'balance parameter'—a measure of the average direction of the kinetic process  $i + j \rightleftharpoons (i + j - 2)$ . This kinetic process is equivalent to a chemical reaction and is called a 'reaction' in the following, to distinguish it from the dynamic processes.  $C$  is the highest cell order in the system,  $p_{i,j}$  is the rate of  $i$ - and  $j$ -cells merging into  $(i + j - 2)$ -cells,  $q_{i,i+j-2}$  the rate of splitting of an  $i$ -cell into  $j$ - and  $(i + j - 2)$ -cells, the  $\delta$ -functions ensure correct counting, and the rightmost sum accounts for the fluctuating number of cells. The unconditional and conditional CODs are assumed to be spatially homogeneous. Rattlers, which are particles that do not transmit forces in the absence of external force fields, are omitted in (1), because they have been shown to affect quasistatic simple-shear dynamics only negligibly [10]. Following our experimental observations below and those in [10],  $Q_{j|i}$  is independent of  $i$  and we omit in the following the conditional notation,  $Q_{j|i} \rightarrow Q_j$ .

At steady state,  $\dot{Q}_k = 0$  for all  $k$ . One possible such state is  $\eta_{i,j} = 0$  for all  $i, j$ , which is the DBSS,  $i + j \rightleftharpoons (i + j - 2)$ . When  $C \geq 6$ , kinetic cycles are possible, in principle [12], supposedly prohibiting this state according to the current paradigm [11]. Yet, Sun *et al.* [13] did observe DBSS in such systems under cyclic shear. This suggests the existence of a fundamental reason for such states, which we now proceed to check analytically.

Since  $Q_{i|j} = Q_i$  at steady state, the probability of  $i$ - and  $j$ -cells being neighbours at time  $t$  is the fraction of the number of such pairs,  $\mathcal{N}_{i,j}$ , out of all possible pairs,

$\mathcal{N} = \bar{z}N/2$ , where  $\bar{z}$  is the mean number of contacts per particle:

$$P_{i,j}(t) = \frac{2\mathcal{N}_{i,j}(t)}{\bar{z}N}, \quad (2)$$

in which  $N$  is the total number of particles and boundary corrections have been neglected. As illustrated in Figs. 1(b)-(d), the number of pairs,  $\mathcal{N}_{i,j}$ , can change in two ways during the reaction,  $k + \ell \rightarrow (k + \ell - 2)$  ( $3 \leq k, \ell, k + \ell - 2 \leq C$ ): (i) both  $i$ - and  $j$ -cells are involved, e.g.,  $i = k$  and  $j = \ell$ ; (ii) only  $i$  or  $j$  is involved. In (i), each such reaction changes  $\mathcal{N}_{i,j}$  by  $\pm 1$ , depending on the reaction direction. For example, in Fig. 1,  $i = k = 3$ ,  $j = \ell = 5$ , and  $3 + 5 \rightarrow 6$ , depleting  $\mathcal{N}_{3,5}$  by one. The net rate of this reaction is  $\eta_{i,j}$  and, therefore, it contributes  $-N_c \eta_{i,j}$  to  $\dot{\mathcal{N}}_{i,j}$ , with  $N_c$  the total number of cells. Case (ii) comprises two sub-cases: (iia)  $i + k \rightleftharpoons (i + k - 2)$  ( $k \neq j$ ,  $3 \leq k \leq C + 2 - i$ ), illustrated in Fig. 1(c); (iib)  $k + (i + 2 - k) \rightleftharpoons i$  ( $k \neq j$ ,  $3 \leq k \leq C$ ), illustrated in Fig. 1(d). In each sub-case,  $\mathcal{N}_{i,j}$  and  $N_c$  change by  $\pm 1$ . The net contribution of these events to  $\dot{\mathcal{N}}_{i,j}$  depends on the difference between the reaction rates,  $\sum_{\ell} \eta_{\ell,i+2-\ell} - \sum_k \eta_{i,k}$ , and on the number of  $i$ - $j$  neighbours,  $\mathcal{N}_{i,j} = P_{i,j} \bar{z}N/2$ . E.g., in Fig. 1, the reaction  $3 + 5 \rightarrow 6$  contributes  $-\bar{z}NP_{4,5}\eta_{3,5}/2$  to  $\dot{\mathcal{N}}_{4,5}$  and  $+\bar{z}NP_{4,6}\eta_{3,5}/2$  to  $\dot{\mathcal{N}}_{4,6}$ . Combining these cases, gives

$$\begin{aligned} \dot{\mathcal{N}}_{i,j} = & -N_c \eta_{i,j} - \frac{\bar{z}NP_{i,j}}{2} \left( \underbrace{\sum_k \eta_{\langle i,k \rangle} - \sum_{\ell} \eta_{\langle \ell, i+2-\ell \rangle}}_{= \frac{\bar{z}NP_{i,j}}{2} (\dot{Q}_i - Q_i \sum_{m,n} \eta_{m,n})} \right) \\ & - \frac{\bar{z}NP_{i,j}}{2} \left( \underbrace{\sum_k \eta_{\langle j,k \rangle} - \sum_{\ell} \eta_{\langle \ell, j+2-\ell \rangle}}_{= \frac{\bar{z}NP_{i,j}}{2} (\dot{Q}_j - Q_j \sum_{m,n} \eta_{m,n})} \right), \end{aligned} \quad (3)$$

in which we have introduced, for simplicity, the notation  $\langle i, j \rangle$ , which orders the indices,  $j > i$  and  $\eta_{\langle i, j \rangle} = 0$  when  $j < i$ . This avoids double counting and allows us to omit the  $\delta$ -functions and the  $1/2$  factor in Eqs. (1). The first term in (3) arises from case (i) and the second and third arise from cases (iia) and (iib), respectively. Only the indices  $i$  and  $j$  change between the second and third terms. In the second term, the reaction  $\eta_{\langle j, k \rangle}$  depletes  $\mathcal{N}_{i,j}$  when  $i + k \rightarrow (i + k - 2)$  and increases it when  $(i + k - 2) \rightarrow i + k$  (case (iia)). The reaction  $\eta_{\langle \ell, i+2-\ell \rangle}$  increases  $\mathcal{N}_{i,j}$  when  $\ell + (i + 2 - \ell) \rightarrow i$  and depletes it when  $i \rightarrow \ell + (i + 2 - \ell)$  (case (iib)). The third term affects  $\mathcal{N}_{i,j}$  similarly. Using Eq. (1), the terms in the brackets of the second and third terms reduce to the expressions written under them. Using then the identity [1]

$$\sum_{\substack{m,n=3 \\ m \leq n \\ m+n-2 \leq C}} \eta_{m,n} = -\frac{\dot{N}_c}{N_c} = -\frac{\dot{\bar{z}}}{\bar{z} - 2}, \quad (4)$$

simplifies (3) to

$$\begin{aligned} \dot{N}_{i,j} = & -N_c \eta_{i,j} + \frac{\bar{z} N P_{i,j}}{2} \left( \dot{Q}_i + Q_i \frac{\dot{\bar{z}}}{\bar{z} - 2} \right) \\ & + \frac{\bar{z} N P_{i,j}}{2} \left( \dot{Q}_j + Q_j \frac{\dot{\bar{z}}}{\bar{z} - 2} \right). \end{aligned} \quad (5)$$

At steady state, all the time derivatives vanish and Eq. (5) reduces to

$$\eta_{i,j} = 0 \quad \forall i, j. \quad (6)$$

We arrived at our destination—every reaction is balanced and these are DBSS! This explains the experimental observations in [13] and in our experiments below. We discuss this surprising result in the concluding section.

**Ramification for maximum-entropy CODs:** It has been shown that, under some conditions, simple shear gives rise to steady states CODs that maximise the entropy under one constraint [10]. The constraint may be the steady-state mean cell order  $\bar{k} = \sum_{k=3}^C k Q_k$ ,  $\bar{z}$ , or  $Q_3$  [14]. Using  $\bar{k}$ , for example, the Lagrangian  $\mathcal{L}$ , which corresponds to the entropy  $S \equiv -\sum_k Q_k \ln Q_k$ , is given by

$$\begin{aligned} \mathcal{L} = & -\sum_{k=3}^C Q_k \ln Q_k - \mu \left( \sum_{k=3}^C Q_k - 1 \right) \\ & - \lambda \left( \sum_{k=3}^C k Q_k - \bar{k} \right), \end{aligned} \quad (7)$$

with  $\mu$  and  $\lambda$  the Lagrange multipliers corresponding to the normalisation and mean constraints, respectively. Maximising with respect to  $\mu$  and imposing the normalisation condition, yields

$$Q_k = \frac{e^{3\lambda} (1 - e^{-\lambda})}{1 - e^{-\lambda(C-2)}} e^{-\lambda k} \equiv A e^{-\lambda k}. \quad (8)$$

Imposing the mean order condition, yields an algebraic equation for  $e^{-\lambda}$ ,

$$\sum_{k=3}^C (k - \bar{k}) e^{-\lambda k} = 0, \quad (9)$$

whose solution yields  $\lambda(\bar{k}, C)$ . The solution can be expressed in terms of the mean coordination number  $\bar{z}$  by using Euler's relation for planar graphs [15]

$$\bar{k} = \frac{2\bar{z}}{\bar{z} - 2}. \quad (10)$$

Eq. (8) together with  $\lambda$  obtained from (9) is the maximum-entropy COD for finite  $C$ , which generalises the one obtained in [10] for  $C \rightarrow \infty$ .

To study the DBSS of systems that maximise the entropy, we substitute (8) in the detailed balance condition,

$$\begin{aligned} \eta_{i,j} &= p_{i,j} Q_i Q_j - q_{i+j-2,i} Q_{i+j-2} \\ &= A e^{-\lambda(i+j-2)} (A p_{i,j} e^{-2\lambda} - q_{i+j-2,1}) = 0, \end{aligned} \quad (11)$$

which yields

$$\alpha_{i,j} \equiv \frac{p_{i,j}}{q_{i+j-2,i}} = \frac{e^{2\lambda}}{A} = \frac{1 - e^{-\lambda(C-2)}}{e^{\lambda} - 1}. \quad (12)$$

This result is significant; the ratio of the cell merging and splitting rates is constant and independent of  $i$  and  $j$ . The COD, which is a key characteristic of the structure, is determined by this one parameter. The procedure is to measure this parameter's value in the experiment or simulation in statistically abundant reactions, determine from it  $\lambda$  by using (12), and then determine  $Q_k$  and  $\bar{k}$ , using (8) and (9).

**Experimental validation:** We tested the above results in rotational shear experiments, using the setup shown in Fig. 2(a). 2410 Acrylonitrile butadiene styrene (ABS) rings of inter-particle friction coefficient  $\mu = 0.46 \pm 0.05$  were assembled on the plate. Four diameters were used to minimise crystallisation: 7mm, 9mm, 11mm, and 14mm of respective number distribution 600, 600, 680, and 530. We chose rings rather than discs to improve particle tracking. The assembly was sheared by peripheral belts at constant speed  $v$  (blue arrows in Fig. 2(a)), giving rise to a Couette-like particle flow. A constant force (red arrows in Fig. 2(a)) was maintained on two opposite boundaries by weights on deflection pulleys. The boundaries were free to move in and out to keep the confining pressure constant. A camera above the system took a photograph every second. Particles were tracked from frame to frame, using an in-house Mathematica-based code. The code was used to find particle positions, identify contacts, obtain the contact network and cell structure, extract the COD and, comparing individual cell orders between consecutive frames, compute the rates  $p_{i,j}$  and  $q_{i,j}$ . Further details are available in the supplemental material [16]. We limited the analysis to a circular region of diameter 1084 pixels, in which the particle velocity profile was proportional to the radius, yielding a constant shear rate [16].

The initial states were prepared by placing the articles arbitrarily within the rectangular area before attaching the weights. To break any contacts and remove incidental correlations, a hair dryer was used to blow air from different directions into the spaces between particles. A confining normal stress of 65.4N/m was then applied to the opposing boundaries and the assembly was sheared at  $v = 1\text{cm/s}$  for 10 minutes to generate the initial state.

From this state, we ran the belts at  $v = 0.2\text{m/s}$  and a pressure of  $p = 32.7\text{N/m}$ . We found that the COD reaches a steady state,  $\dot{Q}_k \approx 0$ , after approximately

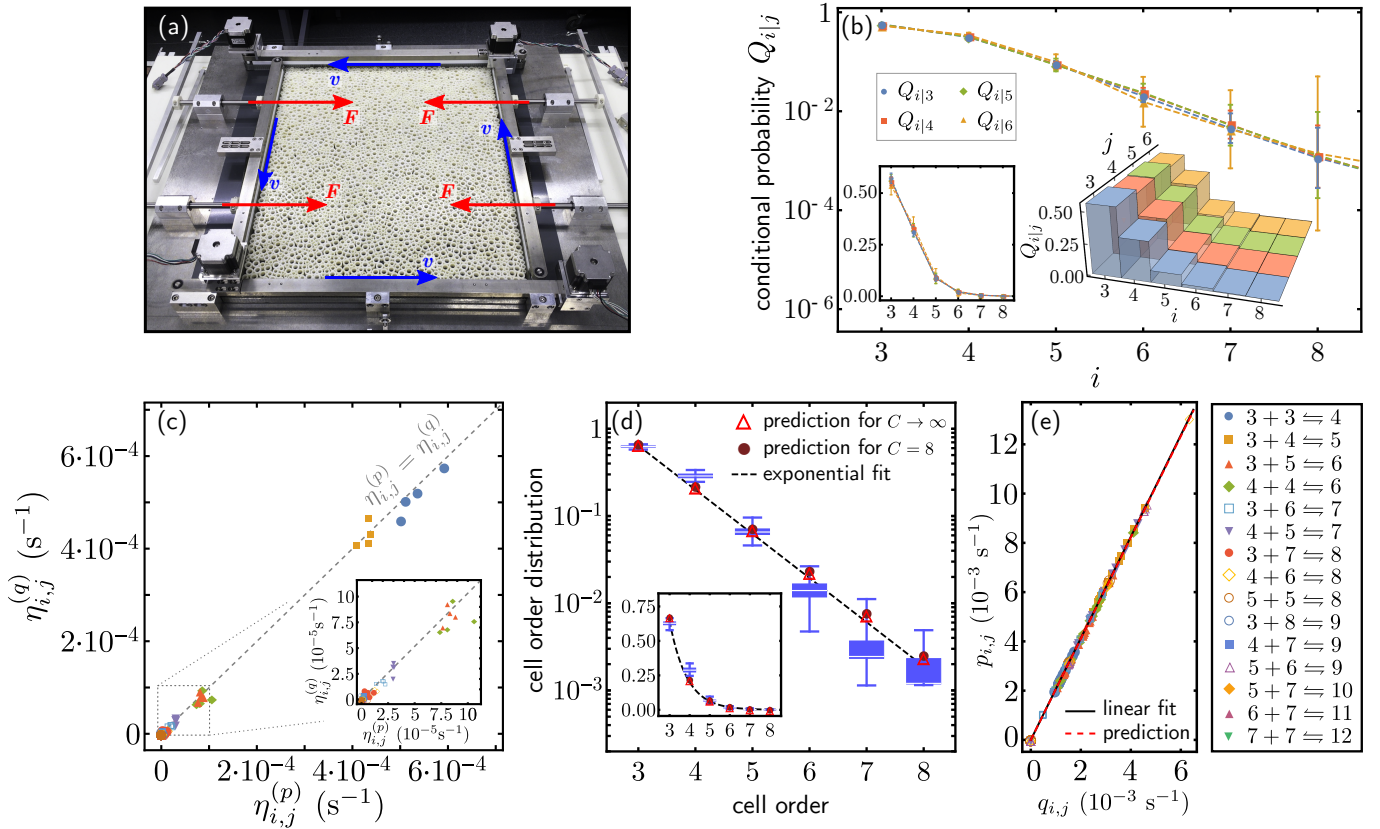


FIG. 2. **The rotational shear experiment.** (a) The experimental setup – an assembly of ABS particles is sheared by the motion of belts running at constant speed  $v$  along the four boundaries (blue arrows). Weights attached via deflection pulleys maintain a constant force  $F$  on two opposite sides (red arrows). (b) The conditional COD – the plots of  $Q_{i|j}$  vs.  $i$  collapse onto one curve for all  $j$ , showing that  $Q_{i|j}$  is independent of  $j$  and every cell sees the same neighbourhood independent of its order. (c) The steady state reaction rates of merging,  $\eta_{i,j}^{(p)}$ , and breaking,  $\eta_{i,j}^{(q)}$ , balance out. (c) Individual data represent the average of  $\eta_{i,j}^{(p)}$  and  $\eta_{i,j}^{(q)}$  during one of the four measurement cycles for all the reactions up to, and including, cells order  $C = 12$ . (d) COD as a function of the cell order. We show the COD data in semi-log scale of 800s of measurement as box plots and compare it to the COD we calculate from the experimental mean cell order  $\bar{k} = 3.48 \pm 0.02$  for  $C = 8$  (red disks) and  $C \rightarrow \infty$  (red triangles). We also show an exponential fit as dashed lines. Theory prediction and experimental data are in good agreement. The fact that we slightly underestimate the fraction of 4-cells in the system may be due to rattlers, or the relatively low friction coefficient which favours smaller cells over the less mechanically stable larger cells. The inset shows the COD on a linear scale. (e) Rates of merging and breaking for different reactions. Each measurement is shown as individual data and the mean for each reaction is shown in the inset. The ratio is the same for all rates because all fall on the same line. The theory prediction for this ratio, Eq. (12), is practically identically with a fit to the experimental data.

60 minutes. We therefore applied shear for 60min and then recorded the measurements for another 60 minutes of which we used the last 800s to obtain data. We repeated this procedure four times for improved statistics. From the images, we constructed the COD and conditional probabilities  $Q_{i|j}$  for each time step. For the rates, we counted contact events over periods of 200s, obtaining 4 data sets for each of the 4 measurement runs, altogether 16 data points for each reaction. From these data we determined the rates  $p_{i,j}$ ,  $q_{i,j}$  and the values of the cell merging rates,  $\eta_{i,j}^{(p)} \equiv p_{i,j}Q_iQ_j$ , and the cell splitting rates,  $\eta_{i,j}^{(q)} \equiv q_{i+j-2,1}Q_{i+j-2}$ .

To check our analysis, we first plot  $Q_{i|j}$  as a function of  $i$  (Fig. 2 (b)) up to  $i = 8$  and  $j = 6$ . In this regime,

we obtain the best statistics. The curves for different values of  $j$  collapse onto a master curve independent of  $j$ , supporting our analysis. Next, we plot the values of  $\eta_{i,j}^{(q)}$  against  $\eta_{i,j}^{(p)}$  (Fig. 2 (c)). To a very good accuracy,  $\eta_{i,j}^{(p)} = \eta_{i,j}^{(q)}$ , namely,  $\eta_{i,j} = 0$  and these are indeed DBSS. The steady state COD is shown in Fig. 2 (d), with the error bars representing the 5% to 95% quantiles. To test if our measured COD maximises the entropy, we used the measured value of  $\bar{k} = 3.480 \pm 0.017$  and both  $C = 8$  or  $C \rightarrow \infty$  in Eqs. (7)-(12) to calculate the exponent of the maximum-entropy exponential COD. For  $C \rightarrow \infty$ , we find  $\lambda = 1.13 \pm 0.03$  and for  $C = 8$ ,  $\lambda_8 = 1.116 \pm 0.026$ . Fitting the experimentally measured values of  $Q_k$  to an exponential, we obtained  $\lambda_{\text{exp}} = 1.17 \pm 0.10$ , which fits

better the  $C \rightarrow \infty$  case. Apart from a small discrepancy at  $Q_4$ , the maximum-entropy COD thus fits well the measured COD.

We calculate the rates  $p_{i,j}$  and  $q_{i,j}$ , by using the fitted COD of Fig. 2 (e) in the normalised expressions

$$p_{i,j} = \frac{n_{i,j}^{(p)}(t, \Delta t)}{Q_i Q_j N_c \Delta t}, \quad q_{i,j} = \frac{n_{i,j}^{(q)}(t, \Delta t)}{Q_{i+j-2} N_c \Delta t}. \quad (13)$$

$n_{i,j}^{(p/q)}$  is the number of merging (breaking) events between  $t$  and  $t + \Delta t$ . These data collapse nicely onto a single line, yielding a constant  $\alpha_{i,j} = 2.05 \pm 0.08$  as predicted from Eq. (12) using the calculated value of  $\lambda_8$ , which is in excellent agreement with the fitted constant of  $\alpha_{i,j} = 2.062 \pm 0.002$ . Here, the fit error is negligible, but mainly comes from propagation of the assumed uncertainty in the rates. The use of the fitted COD for calculating  $p_{i,j}$  and  $q_{i,j}$ , rather than the raw data, is to alleviate the small statistics problems for larger cell orders. Fluctuations in the COD are amplified when calculating the rates due to the division by  $Q_i$ . Many more experimental runs would be needed to obtain a reliable result directly from the COD data (for more details on this issue, see supplemental material [16]). Nevertheless, using the experimental  $\eta_{i,j}^{(p/q)}$  and the fitted COD to obtain Fig. 2 (e), we see a remarkable agreement with the theory prediction.

**Conclusions:** To conclude, we showed analytically that when the cell order distribution (COD) around a cell in quasistatic dynamics is independent of its order, then the steady states of those dynamics satisfy detailed balance. This result explains the observations of non-equilibrium detailed balance steady states (DBSS) in [13] and it is supported by our experiments in systems driven differently—by rotational shear. This suggests that DBSS extend beyond cyclic and rotational shear and may be the norm rather than an exception.

We further showed that, if the COD in such systems also maximises the entropy [10], then the steady state CODs are governed by only one parameter—the ratio of cell merging and breaking in any arbitrary reaction,  $\alpha = p_{i,j}/q_{i+j-2,i}$ , which is independent of  $i$  and  $j$ .

These results are significant. Firstly, they call into question the existing paradigm that detailed balance can only arise in equilibrium systems and that kinetic processes in non-equilibrium steady states can only be balanced by cycles, such as  $A \rightarrow B \rightarrow C \rightarrow A$ . Secondly, the identification of a single parameter governing the steady states makes it possible to construct new models of such dynamics with a reduced number of parameters, potentially including considerations of entropy and stability [10]. Thirdly, the detailed balance principle had an enormous impact on the development of equilibrium physics and the discovery of this principle in a wide range of granular systems could lead to a similar avalanche of new results.

**Acknowledgements:** We thank Karolina Zeh and Martin Müller for assisting with designing and building the experimental setup.

---

\* clara.wanjura@mpl.mpg.de

† rbb11@cam.ac.uk

- [1] C.C. Wanjura, P. Gago, T. Matsushima, R. Blumenfeld, *Granular Matter* **22**, 91 (2020).
- [2] T. Matsushima, R. Blumenfeld, *Phys. Rev. Lett.* **112**, 098003 (2014).
- [3] T. Matsushima, R. Blumenfeld, *Phys. Rev.* **E 95**, 032905 (2017).
- [4] S.F. Edwards, R.B. Oakeshott, *Physica* **D 38**, 88 (1989).
- [5] H.-J. Vogel, K. Roth, *J. Hydrol (Amsterdam, Neth.)* **272**, 95 (2003).
- [6] G. Cheng, A. Yu, P. Zulli, *Chem. Eng. Sci.* **54**, 4199 (1999).
- [7] T. Aste, T. Di Matteo, M. Saadatfar, T.J. Senden, M. Schroter, H.L. Swinney, *Europhys. Lett.* **792**, 24003, (2007).
- [8] S. Meyer, C. Song, Y. Jin, K. Wang, H. A. Makse, *Physica* **A 389**, 5137 (2010).
- [9] R.C. Ball, R. Blumenfeld, *Phys. Rev. Lett.* **88**, 115505 (2002).
- [10] X. Sun, W. Kob, R. Blumenfeld, H. Tong, Y. Wang, and J. Zhang, *Phys. Rev. Lett.* **125**, 268005 (2020).
- [11] M. J. Klein, *Phys. Rev.* **97**, 1446 (1955)
- [12] The only possible reactions for  $k < 6$  which cannot give rise to cycles according to the master equations (1) are  $3 + 3 \rightleftharpoons 4$  and  $3 + 3 \rightleftharpoons 5$ . For higher maximal cell orders, cycles are possible. For instance, for  $k < 7$ , we have  $3 + 3 \rightleftharpoons 4$ ,  $3 + 4 \rightleftharpoons 5$ ,  $3 + 5 \rightleftharpoons 6$  and  $4 + 4 \rightleftharpoons 6$ , which, in principle, would admit the cycle  $3 + 5 \rightarrow 6 \rightarrow 4 + 4 \rightarrow 6$ .
- [13] X. Sun, Y. Wang, Y. Wang, R. Blumenfeld, and J. Zhang, Experimental evidence of detailed balance in granular systems, arXiv:2105.01355 (2021).
- [14] R. Blumenfeld, Disorder Criterion and Explicit Solution for the Disc Random Packing Problem, *Phys. Rev. Lett.* **127**, 118002 (2021).
- [15] See, e.g. R. Blumenfeld, S. F. Edwards, S. M. Walley, *Granular systems*, in *The Oxford Handbook of Soft Condensed Matter*, Eds. E.M. Terentjev and D.A. Weitz, (Oxford University Press, Oxford, UK, 2015).
- [16] The SM contains further details on the analysis of the experimental data.

## Detailed balance in non-equilibrium dynamics of granular matter: derivation and implications —Supplementary Material—

**Subsystem with constant shear rate:** Since the experimental system is sheared on all sides, the particles follow approximately circular trajectories and their velocities are rotationally symmetric with respect to the centre. We only analyse the part of the system with approximately constant shear rate / azimuthal velocity component (AVC). To identify this regime, we analysed the particle AVCs at different radii from the centre. First, we obtained the centre by fitting the function

$$v(x, y) = v_0 + a((x - x_0)^2 + (y - y_0)^2) + b\sqrt{(x - x_0)^2 + (y - y_0)^2} + c$$

to the 2 dimensional velocity data  $v(x, y)$ . To this end, we used the data from all time frames. This function is rotationally symmetric with respect to  $(x_0, y_0)$ , which is the centre of the rotation, see Fig. S1(a).

Next, we analysed the AVC as a function of time. The AVC of a particle does not stay constant, but rather, particles are accelerated and decelerated in response to changes in the local forces and the structure, see Fig. S1(b). It is plausible that this velocity's maximum is correlated with the shear rate. Since the maximum is relatively noisy, we used the 95% quantile of the AVC for our analysis and we plot it as a function of the radius in Fig. S1(c). The plot substantiates that there is a regime  $0 \leq r \leq r_0 = 542$  pixels over which  $v(r)$  is linear. In this region  $\partial v(r)/\partial r \equiv \text{constant}$  and it is therefore this region that we used for our analysis.

**Contact detection:** Two particles,  $j$  and  $k$ , were considered in contact when their centroids,  $(x_{j,k}, y_{j,k})$ , and radii,  $r_{j,k}$ , obeyed

$$(x_j - x_k)^2 + (y_j - y_k)^2 \leq (r_j + r_k + d)^2 \quad (\text{S1})$$

with  $d$  an additive constant that effectively enlarges the particle radius to make them overlap. The optimal value of  $d$  was determined by running the image analysis for different values of  $d$  and counting the number of detected contacts in the system. Increasing  $d$ , particles start coming into contact at some value  $d_c$  and the number of detected contacts increases sharply. Thereafter, the number of contacts increases more slowly (and seemingly linearly), as more and more false contacts are detected. This is shown in Fig. S2(a). We defined the optimum value of  $d$  slightly to the right of the initial sharp

increase in the number of contacts to eliminate the error originating from the detection of false contacts. Practically, this means that we chose the smallest value of  $d$  for which the second derivative of the number of detected contacts vanishes, see Fig. S2(b). This value is  $d = 0.5$ .

**Detecting events and clapping:** As reported in simulations [1], pairs of particles can ‘clap’, namely, make and break contact repeatedly. We also observed clapping in these experiments. This phenomenon does not change the balance of reactions and therefore neither affects the observation of the detailed balance in steady states,  $\eta_{i,j} = 0 \forall i, j$ . Clapping takes place in the experiment on relatively well-defined time scales. On making contact, momentum can drive the two particles slightly apart until the compressive force field pushes them into contact again. This can be repeated until this kinetics is damped. This separation of scales allowed us to filter out such events by removing any events involving the same two grains that happen within a certain time duration  $\tau$ . In our analysis, when a pair of particles clap during any time shorter than  $\tau$ , this is counted as one event if the number of claps is odd, in which case the final structure has changed. Otherwise the contact state of the two particles is deemed unchanged. An illustration of this process is shown in Fig. S2(c). Initially, particles make and break contact rapidly and eventually settle. Later events are well separated in time from the initial clapping. To determine  $\tau$ , we plot the number of detected events as we vary  $\tau$  (Fig. S2(d)). This function decreases faster than linearly when clapping is involved and transitions into a linear decrease when non-clapping events starts to be filtered out. The transition is at  $\tau = 15\text{sec}$ , which is therefore the optimal value for filtering out only the clapping events.

**Rates ratios:** We calculate the rates from the number of merging  $p_{i,j}$  and breaking  $q_{i+j-2,i}$  events  $n_{i,j}^{(p/q)}$ , see Eq. (13). The values of the fractions,  $Q_k$  were obtained from the exponential fit, shown in Fig. 2 (d) in the main text rather than directly from the cumulative experimental data during  $\Delta t$ , which includes unavoidably large fluctuations. These large fluctuations propagate to the rates and are amplified due to the division by  $Q_k$ . For completeness, we provide the plot with reactions up to  $C = 6$  in Fig. S3.

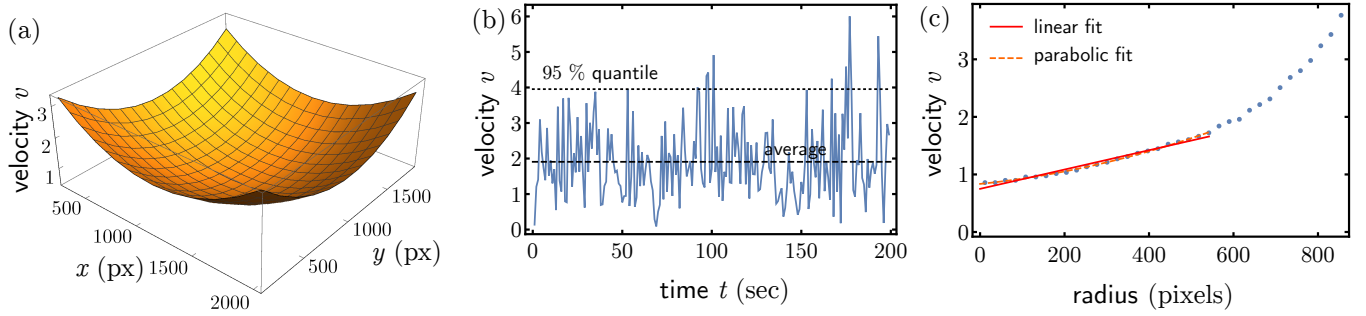


FIG. S1. **Particle AVCs and the region of constant shear rate.** (a) We obtain the system's centre through a parabolic fit to the AVC data. (b) Representative example of a particle AVC. Characteristically, particles move in jolts rather than at constant speed. The 95 % quantile represents the maxima of these peaks and it is these values that we relate to the shear rate, rather than the mean. (c) 95 % quantile of the velocity as a function of the distance to the system centre (radius). Up to a radius  $\leq 546$  pixels, there is a linear regime, in which the parabolic and linear fits hardly differ.

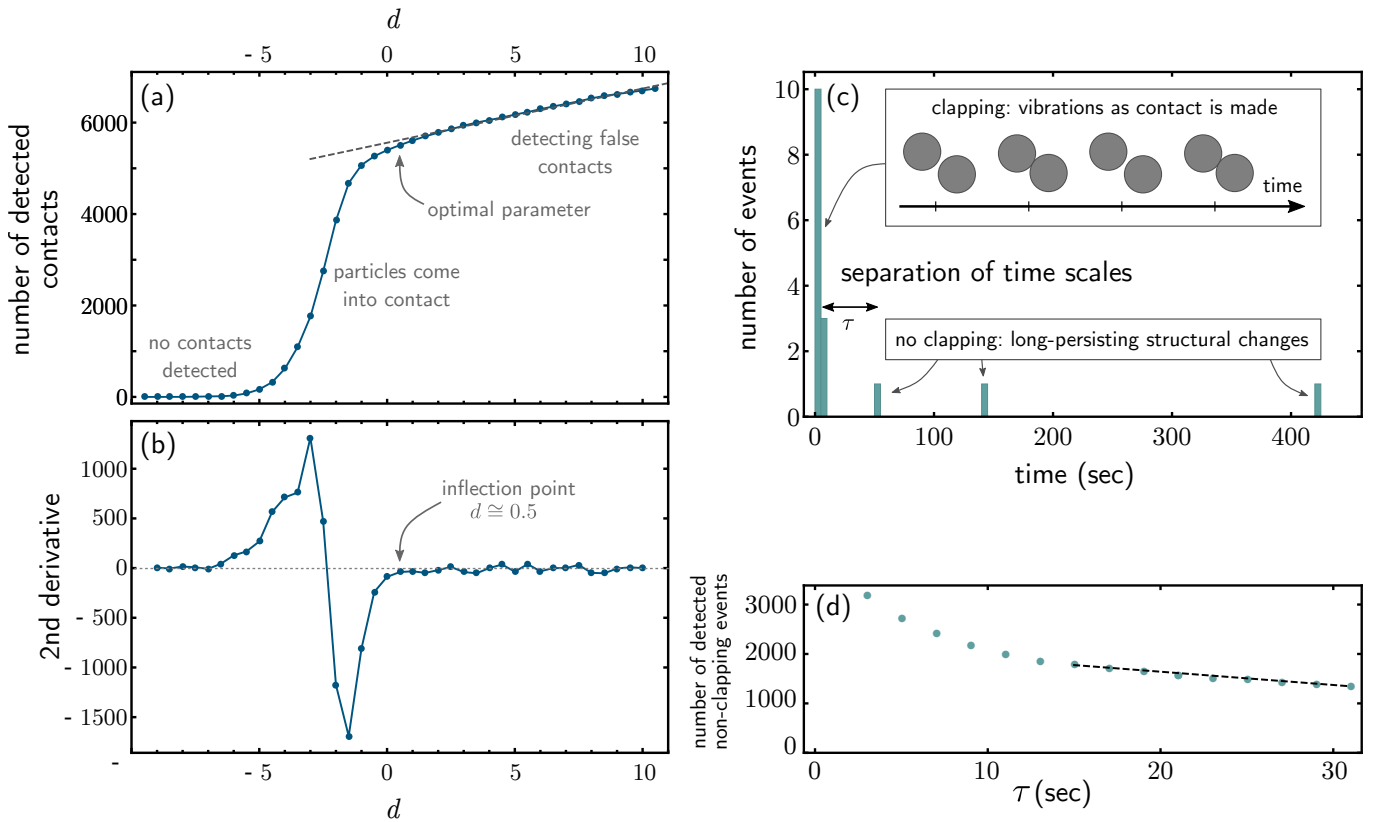


FIG. S2. **Contact detection and detecting structure-changing contact events.** (a) The number of detected contacts as a function of the detection parameter  $d$ . The sharp increase in the number of particles, when they start coming into contact, is followed by a slow, approximately linear, increase (grey dashed line). The slow increase is the result of falsely detected contacts. The optimal choice of  $d$  is immediately to the right of the sharp increase, just before the linear increase and when the second derivative shown in (b) vanishes. This value is  $d = 0.5$ . (c) Residual kinetic energy can result in vibrations of particles, causing repeated making and breaking of a contact between them. Clapping takes place typically on a time scale  $\leq \tau$  that is shorter than non-clapping events. (d) The number of detected events drops rapidly with and then settles into a linear decrease beyond  $\tau = 15$ sec. This is when the number of non-clapping contacts start to be filtered out and therefore is the optimal value for filtering out only clapping events.

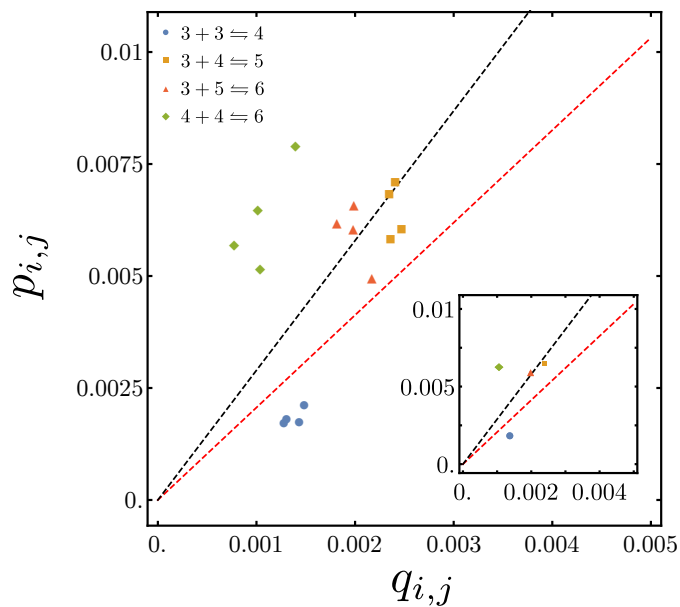


FIG. S3. **Rates ratios calculated from COD data.** Rather than using the fitted COD shown in Fig. 2(h), we divide by the mean COD during the respective time interval during which we count the contact events. This leads to a broader distribution of the data, and a discrepancy between a linear fit to the data (black dashed line) and the theory (red dashed line) due to rattlers and boundary effects.